phys. stat. sol. (c) **1**, No. 5, 1097–1114 (2004) / **DOI** 10.1002/pssc.200304315

The physics and technological aspects of the transition from amorphous to microcrystalline and polycrystalline silicon

J. Kočka[*, 1], **A. Fejfar**[1], **T. Mates**[1], **P. Fojtík**[1], **K. Dohnalová**[1], **K. Luterová**[1], **J. Stuchlík**[1], **H. Stuchlíková**[1], **I. Pelant**[1], **B. Rezek**[1, 2], **A. Stemmer**[2], and **M. Ito**[3]

[1] Thin Films Department, Institute of Physics AS CR, Cukrovarnická 10, 162 53 Prague, Czech Republic
[2] Nanotechnology Group, Swiss Federal Institute of Technology, Tannenstr. 3, 8092 Zurich, Switzerland
[3] Toppan Printing Co., 4-2-3 Takanodai-Minami, Sugito machi, Kita Katsushika, Saitama, Japan

Received 4 December 2003, revised 19 December 2003, accepted 22 December 2003
Published online 18 March 2004

PACS 61.43.Dq, 68.37.–d, 73.63.Bd, 84.60.Jt, 85.30.De

Silicon thin films grown near the boundary between the amorphous/microcrystalline growth offer superior properties for industrial applications. Series of silicon samples, in which crossing of this transition region was achieved by changing a single technological parameter (dilution of silane in hydrogen, deposition temperature, sample thickness) were used to test our model of transport, connecting the macroscopically observed transport properties and the crystallinity, hydrogen content, grain size and grain boundaries. Microscopic study by AFM led to the formulation of the geometrical model of growth of mixed phase Si. The demand for research of microcrystalline or polycrystalline silicon prepared at low substrate temperatures is stimulated by the use of cheap plastic substrates. In addition to a direct deposition an alternative technology, such as metal-induced crystallization supported by the electric field is discussed. Possible future application of thin silicon films, for example in a "nanolithography", is also shown.

1 Introduction

Amorphous hydrogenated silicon (a-Si:H) today belongs among important industrial materials, first of all due to large area matrix of a-Si:H field effect transistors, controlling LCD flat panel displays, as well as due to its use in photovoltaic (PV) solar cells. However, advantages of crystalline forms of thin film silicon, like resistance of nano(micro)crystalline hydrogenated silicon (μc-Si:H) against the light induced degradation or the higher mobility of polycrystalline silicon (poly-Si) attracted lot of researchers to these new materials.

The possibility of depositing Si thin films on flexible plastic substrates is a prerequisite for large variety of new applications of a-Si:H and μc-Si:H and this stimulated our recent research. However, the properties of common plastic substrates limit the deposition to substrate temperature $T_S < 100\,^{\circ}C$. There are generally two ways how to prepare μc-Si:H or poly-Si at low T_S, either by direct deposition, for example [1] by plasma enhanced chemical vapor deposition (PECVD), or by deposition of a-Si:H and its subsequent crystallisation.

Many efforts have been directed towards developing various approaches for crystallization of a-Si:H films, for example by solid-phase crystallization [2], excimer laser annealing [3, 4] or furnace annealing [5–8]. However, the temperature for common furnace crystallization of a-Si:H films must reach at least 600 °C and this is not compatible with low-cost glass or plastic substrates.

In this article we first review many interesting aspects of a-Si:H/μc-Si:H transition with an emphasis to low substrate temperatures ($T_S < 100\,^{\circ}C$), and technological and application related aspects of the

* Corresponding author: e-mail: kocka@fzu.cz, Phone: +420 220 318 449, Fax: +420 233 343 184

μc-Si:H growth. Finally we illustrate an alternative way of preparation of polycrystalline Si at low T_S by transversal electric-field-assisted Metal-Induced Solid Phase Crystallisation (MISPC) and the possibility of using a-Si:H for "nanolitography".

2 Experimental details

We present the results on 4 series of samples, for which a-Si:H/μc-Si:H transition is achieved by changing of one technological parameter. The first series of thin silicon samples [9] has been prepared by PECVD at a very high frequency of 54 MHz, at T_S = 60 °C and with the H dilution (r_H = [H_2]/[SiH_4]) changing from 26 to 167. The second series [1, 10] has been prepared also at 54 MHz but at T_S = 80 °C with the dilution r_H changing from 34 to 168. The third (thickness) series [1] has been prepared at 54 MHz, T_S = 75 °C and r_H = 29 with the thickness changing from 40 nm to 1000 nm and the last series [10, 11] at 54 MHz and high dilution (r_H = 134) in a wide range of temperatures 35 °C $< T_S <$ 200 °C. The thickness of samples was around 400 nm for the first series, around 1000 nm for the second and around 350 nm for the last series.

For crystallisation experiments the a-Si:H films have been deposited at 13.56 MHz from SiH_4 diluted strongly with helium. The substrate temperature T_S was kept as low as 50 °C. For experiments with formation of the charge patterns by the atomic force microscope (AFM) tip the a-Si:H films has been deposited at 13.56 MHz and T_S = 250 °C with the dilution r_H = 11.5.

For evaluation of the crystalline fraction (X_C) the Raman spectroscopy has been used. Coplanar contacts have been used for measurement of the room temperature dc dark conductivity (σ_D), its temperature dependence as well as for photoconductivity (σ_{PH}) and the steady-state photocarrier grating (SSPG) method, from which the ambipolar diffusion length parallel to the substrate (L_{diff}) can be evaluated. H content was determined by elastic recoil detection analysis (ERDA) [12]. For evaluation of roughness we have used our modified AFM [13] by which we measure simultaneously both surface topography and a local current map. More details of the different evaluation techniques are in [10].

3 Physics of a-Si:H/μc-Si:H transition, the role of H and grain boundaries

Since the first demonstration of the fully μc-Si:H solar cell [14] this material is one of the most studied forms of thin film silicon. Different groups have shown that the best solar cells (both a-Si:H and μc-Si:H based) are prepared near the a-Si:H/μc-Si:H transition region.

We have initially studied this transition on μc-Si:H samples, in which the transition naturally appears with the increasing thickness. The results, related mainly to transport properties of μc-Si:H, have been recently summarized in [10]. Our proposed model of transport [15], verified also for a-Si:H/μc-Si:H superlattices [16], is based on the measurements of the dc coplanar dark conductivity, in particular its activation energy E_A and prefactor σ_0, Raman spectroscopy, which allowed us to evaluate the crystallinity, and AFM morphology (RMS roughness).

The basic idea, schematically illustrated in Fig. 1, is the following. It is well known that most of the μc-Si:H contains grains with sizes from few nm (as observed from X-ray diffraction) up to hundreds of nm (evident in microscopical images). We assume that small grains ($10 - 30$ nm) and also their boundaries are nearly defect-free. Whatever is their nature – remaining a-Si:H tissue or tilted boundaries [17] – these boundaries present no barrier for band-like electron transport.

On the other hand we assume that when "large grains" ($100 - 300$ nm large, sometime labelled as "columns") are formed, most of the defects and impurities like O, N, C [18], as well as H, segregate to these boundaries, formed by a-Si:H tissue, whose mobility gap is increased by alloying. Therefore the potential barrier formed at such grain boundaries (see the shifted E_C in Fig. 1) limits the band-like transport and the dominant transport path is forced down to hopping through the tail states below the mobility edge E_C.

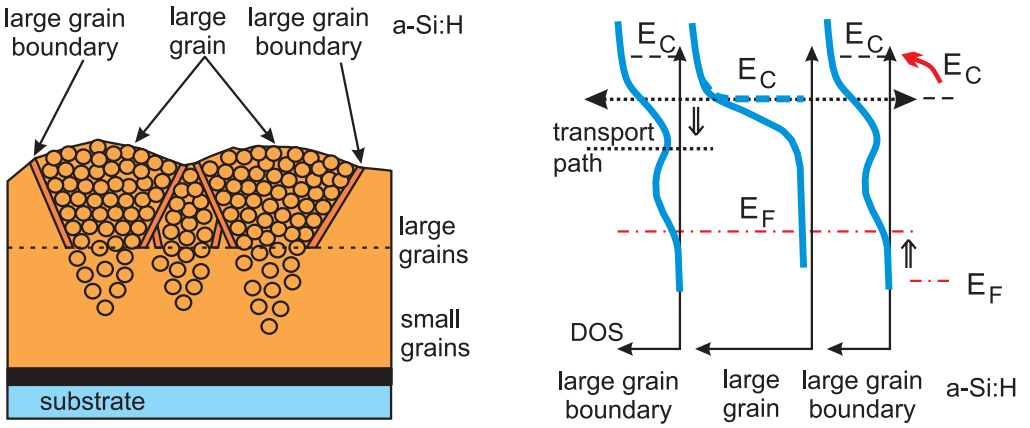

Fig. 1 Schematic drawing of the μc-Si:H film structure and the density of states – N(E) in different parts of the sample as a basis of our model of transport in μc-Si:H, see text (E_F – Fermi level, E_C – conduction band edge).

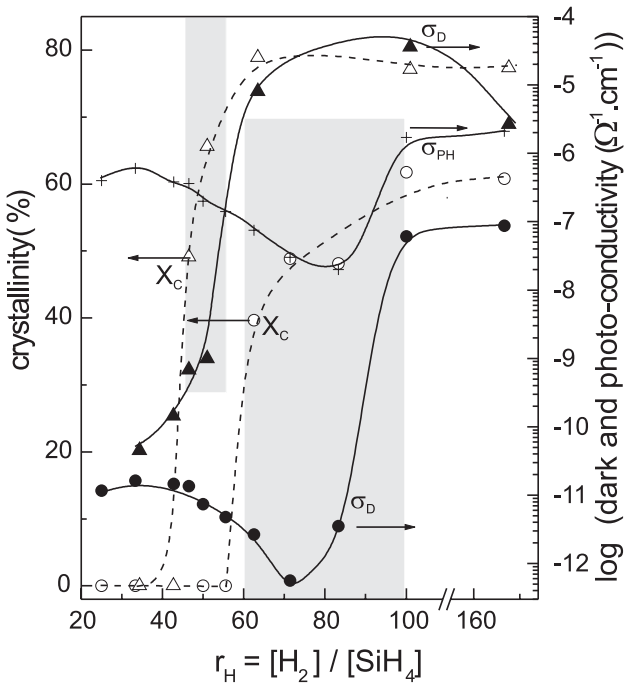

Fig. 2 Crystallinity X_C (open symbols) together with room temperature dark conductivity σ_D (full symbols) of two series of thin silicon films (prepared at $T_S = 60\,^{\circ}$C (circles) and $T_S = 80\,^{\circ}$C (triangles) [1, 9, 10]), together with the photoconductivity (crosses) of $T_S = 60\,^{\circ}$C sample series as a function of the dilution ratio r_H. The lines are added as guides for the eye.

This model is supported for example by ESR results [19]. When the columns are formed in a μc-Si:H, the transport is often anisotropic [10].

Here we will test on few low T_S sample series whether this model is relevant also to these samples and what is the role of H and grain boundaries within and outside the a-Si:H/μc-Si:H transition region.

The transition region is usually defined by the drop of room temperature dark conductivity (typically below $10^{-7}\,\Omega^{-1}\mathrm{cm}^{-1}$) as well as crystallinity drop (X_C — typically below 40 %) [10]. In Fig. 2 there are the results for two dilution series, prepared at T_S = 60 °C and T_S = 80 °C [1, 9, 10].

While for the T_S = 80 °C series the transition region is rather sharp and narrow (see shadowed region in Fig. 2 for $45 < r_H < 56$), for T_S = 60 °C series quite substantial difference between conductivity and crystallinity drops is observed at $61 < r_H < 100$ (marked again as shadowed region in Fig. 2). Interesting is a clear minimum in photoconductivity (σ_{PH}) just in a transition region. Both for a-Si:H and μc-Si:H it is generally accepted that the decrease of the σ_{PH} is related to the increase of the number of defects (see for example [20, 21]). This is actually in good agreement with our assumption that the defects concentrate to the (large) grain boundaries.

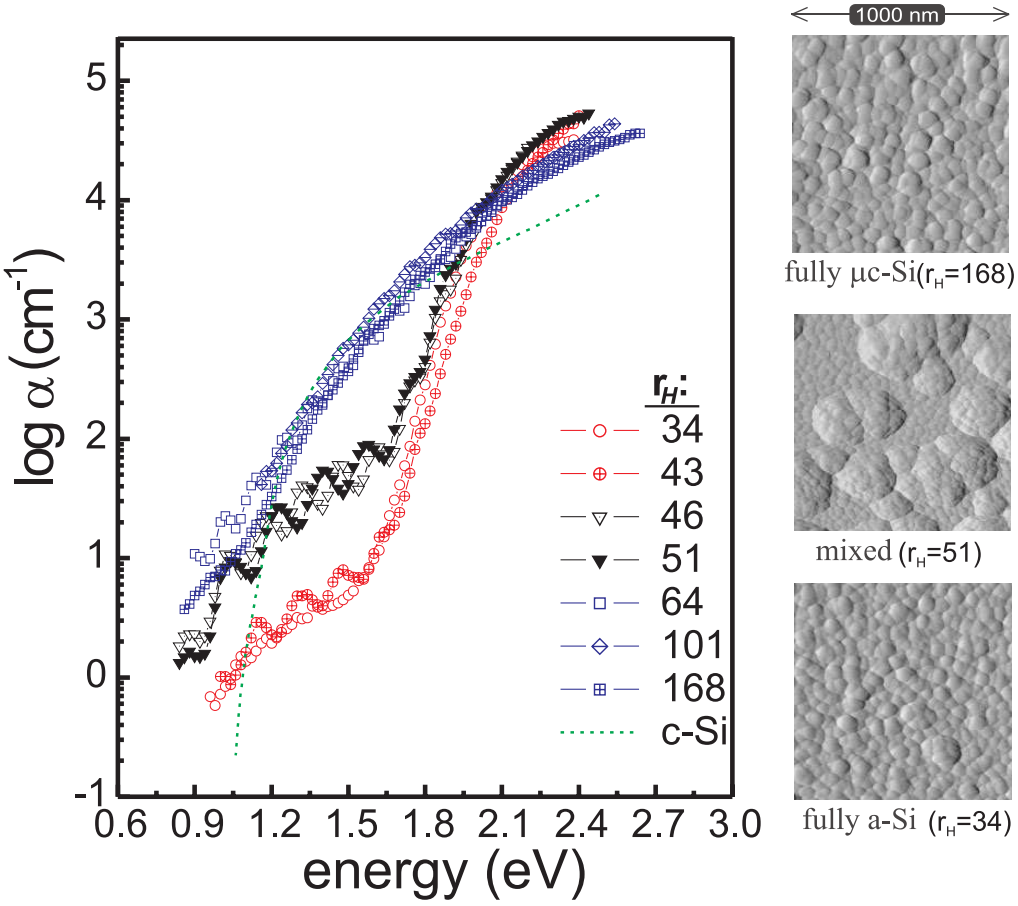

Fig. 3 Absorption coefficient (α), measured by CPM for the T_S = 80 °C sample series as a function of the dilution ratio r_H. AFM topography is shown for selected samples, illustrating the relation to CPM curves.

Direct experimental support to "generally accepted notion" is in Fig. 3, where it is for the T_S = 80 °C dilution series seen that in the region of transition ($r_H \cong 51$) the large grains are clearly formed (see the topography in right-hand part of Fig. 3) and the defect controlled region ($1.2 - 1.5$ eV) of the constant photocurrent method (CPM) curves increases. We have to remark that this increase could be in principle

also due to the increase of the crystalline fraction (before transition to fully microcrystalline state), but then a decrease of α above 2 eV should be observed in parallel, and this is not the case.

In addition to the results shown in Figs. 2 and 3 for the T_S = 80 °C dilution series we have evaluated for this series from SSPG measurement the diffusion length and from AFM topography the RMS roughness. For both of them we have found within the transition region, marked by the shadow in Fig. 4(a), a sharp peak at $r_H \cong 51$. The peak in L_{diff} in the transition region, in which for the T_S = 60 °C series a minimum of σ_{PH} has been observed (see Fig. 2), might be a bit surprising and this is discussed below.

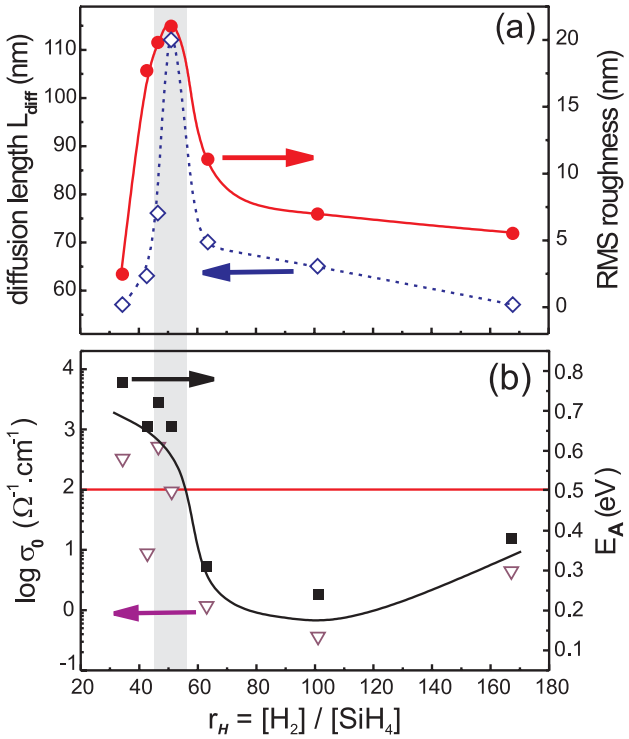

Fig. 4 Diffusion length L_{diff} from SSPG and surface RMS roughness (a) for the $T_S = 80\,°C$ sample series together with the values of room temperature dark conductivity prefactor σ_0 and activation energy E_A (b) as a function of the dilution ratio r_H. For the meaning of the horizontal line at $\sigma_0 = 100\,\Omega^{-1}\mathrm{cm}^{-1}$ and $E_A = 0.5$ eV see text.

The drop of conductivity and crystallinity – together with the topography – illustrated fact (see Fig. 3 and for full series of AFM topography see [1]) that c-Si grains just started to touch at $r_H \cong 51$ which indicates the presence of a percolation threshold. Having in mind our model of transport [15] the question arises whether the percolation threshold is related to formation of "large grains", for which a typical feature is the drop of the conductivity prefactor σ_0 below $100\,\Omega^{-1}\mathrm{cm}^{-1}$ and of the activation energy E_A to below 0.5 eV. Fig. 4(b) displays σ_0 and E_A evaluated recently as a function of r_H for the T_S = 80 °C series. Clearly large grains are formed also in the transition region.

Recently we have studied in detail the "temperature series", prepared at r_H = 134 in a wide range of temperatures 35 °C<T_S < 200 °C. Fig. 5 shows the conductivity and crystallinity for this series as a function of the T_S.

With decreasing T_S from 200 °C to 100 °C the conductivity decreases, then it starts to rise again and finally drops below a typical value of $\sigma_D \approx 10^{-7}\,\Omega^{-1}\mathrm{cm}^{-1}$ at about 60 °C. Moreover, for $T_S < 60\,°C$ the

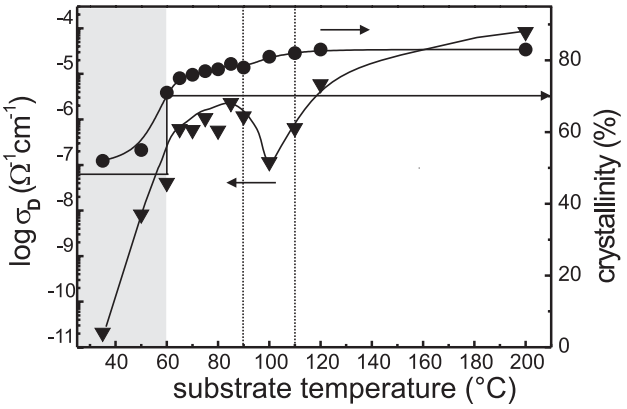

Fig. 5 Room temperature dark dc conductivity σ_D together with crystallinity X_C of sample series, prepared at 54 MHz and high dilution ($r_H = 134$) as a function of the substrate temperature T_S.

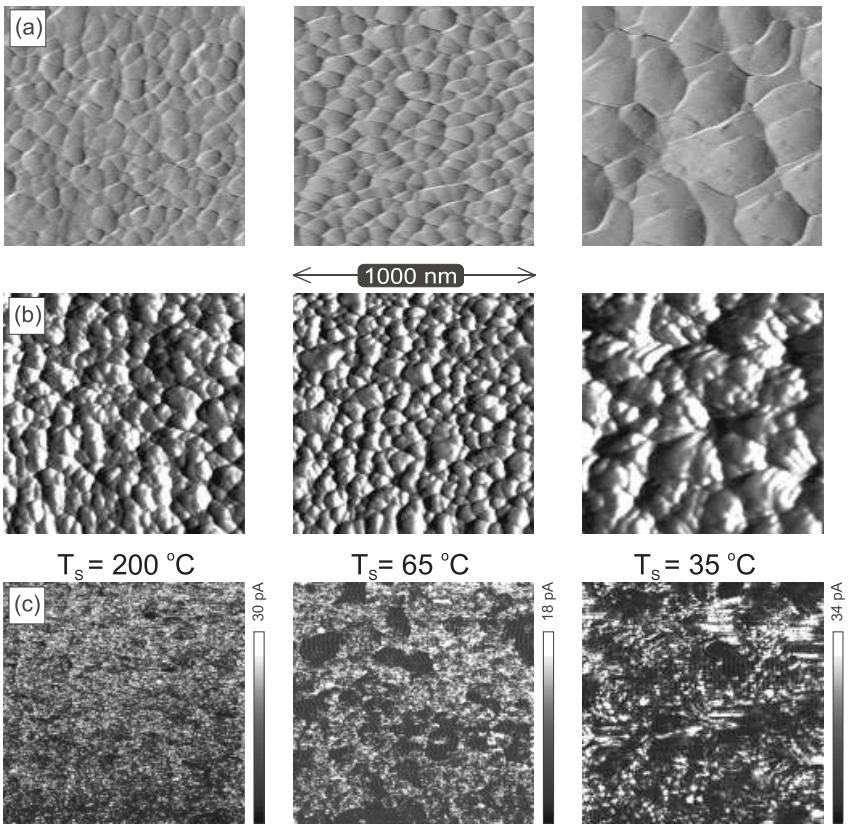

Fig. 6 Surface topography taken by air AFM microscope (a) and UHV-AFM topography (b) combined with the map of local currents (c) of 3 thin silicon samples deposited at 54 MHz and high dilution ($r_H = 134$) and substrate temperatures $T_S = 200\,°C$, 65 °C and 35 °C.

crystallinity drops below 70 % and the roughness (see below) starts to rise — all these facts indicate that there is the a-Si:H/μc-Si:H transition region for $T_S < 60\,°C$, marked by shadowing.

To understand what is going on we have measured AFM topography combined with the maps of local currents [11, 13, 22] for this series, see Fig. 6.

The real surprise was the air AFM topography of the sample prepared at $T_S = 35\,^{\circ}C$, see Fig. 6(a), indicating "large crystallites". Indeed (see Fig. 5) more than 50% crystallinity was later confirmed. The topography measured by UHV-AFM, see Fig. 6(b), is not influenced by the surface adsorbates and gives much better resolution: for the $T_S = 35\,^{\circ}C$ sample it illustrates that "large crystallites" are actually composed of smaller ones. Very interesting results are seen from the maps of local currents, see Fig. 6(c), in which white regions represent more conductive crystalline parts and black ones much less conductive amorphous tissue [13].

It can be seen that even UHV-AFM topography does not precisely describe the real microstructure. The $T_S = 200\,^{\circ}C$ sample is formed by a lot of tiny crystallites, feature typical for high H_2 dilution. For the $T_S = 65\,^{\circ}C$ sample an increased content of amorphous tissue is already evident and in $T_S = 35\,^{\circ}C$ sample the crystallites are mostly isolated by amorphous tissue. This explains why for the $T_S = 35\,^{\circ}C$ sample, even with 50% crystallinity the transport properties are controlled by amorphous tissue, see Fig. 5.

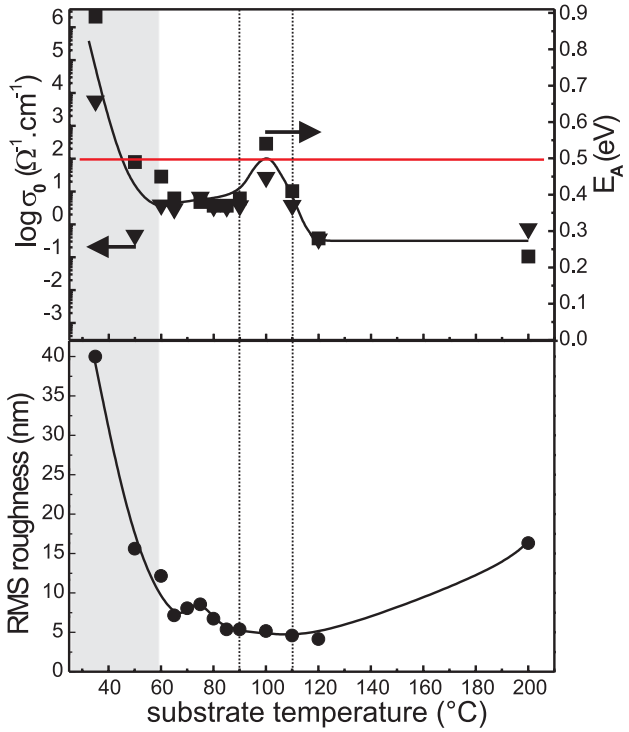

Fig. 7 Surface RMS roughness (bottom) together with values of the conductivity prefactor σ_0 and of the activation energy E_A (top) of sample series, prepared at 54 MHz and high dilution ($r_H = 134$) as a function of the substrate temperature T_S. For the meaning of the horizontal line at $\sigma_0 = 100\,\Omega^{-1}\mathrm{cm}^{-1}$ and $E_A = 0.5$ eV see text.

However, what is the reason for a minimum of conductivity in Fig. 5 in the region $90\,^{\circ}C < T_S < 110\,^{\circ}C$, marked by vertical dotted lines? In Fig. 7 there are RMS roughness and the conductivity activation energy E_A and prefactor σ_0. Increasing roughness for $T_S < 60\,^{\circ}C$ confirms, in agreement with results in Fig. 5, that there is the a-Si:H/μc-Si:H transition region for $T_S < 60\,^{\circ}C$, marked by shadowing again.

In agreement with our model of transport (see above and reference [15]) the drop of prefactor σ_0 to below $100\,\Omega^{-1}\mathrm{cm}^{-1}$ and activation energy E_A below 0.5 eV (see Fig. 7) on the edge of the transition region confirm that the "large grain boundaries (LGB)" are formed. Actually in all samples for $T_S > 60\,^{\circ}C$,

except the $T_S = 100\,°C$ sample, the condition for LGB formation ($\sigma_0 < 100\,\Omega^{-1}cm^{-1}$ and $E_A < 0.5$ eV) is fulfilled. The sample prepared at $T_S = 100\,°C$ is the only sample outside the transition region, for which values of σ_0 and E_A indicate no LGB. So why is this sample exceptional?

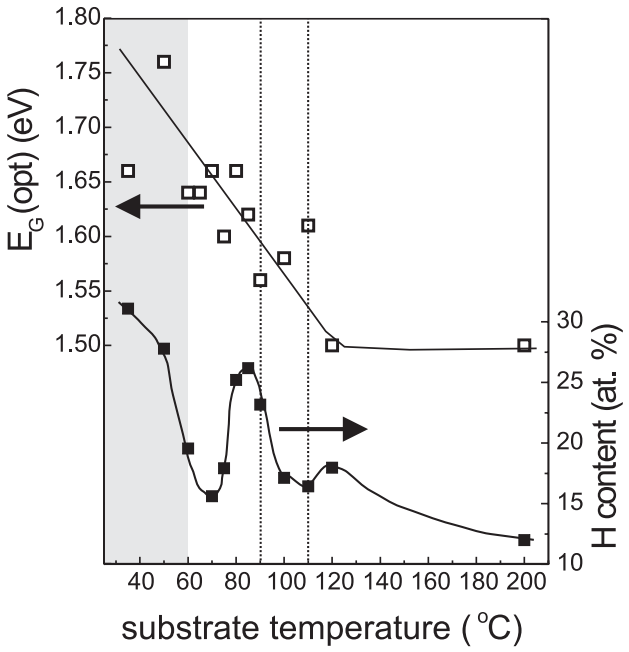

Fig. 8 Optical gap E_G(opt) and hydrogen content from ERDA of the sample series, prepared at 54 MHz and high dilution ($r_H = 134$) as a function of the substrate temperature T_S.

In addition to the peaks of diffusion length and of roughness in a-Si:H/μc-Si:H transition region usually the peak in H content is observed, too [12]. Clear increase of H content for $T_S < 60\,°C$, see Fig. 8, is the last confirmation that really for $T_S < 60\,°C$ there is the a-Si:H/μc-Si:H transition region.

However, the H content dependence on substrate temperature in Fig. 8 shows another interesting feature — a sharp maximum at $T_S \cong 85\,°C$ and a smaller one at $T_S \cong 120\,°C$! In the same figure there is the optical gap, which for $T_S < 120\,°C$ smoothly increases from 1.5 to 1.75 eV. The complicated behavior of H content, while its average increases similarly to optical gap, has one simple explanation — H fluctuations are concentrated to narrow space (and the natural candidate are the grain boundaries) so that volume averaged optical properties are not so influenced by these fluctuations.

Basic idea of our model of transport is that formation of LGB is connected to the potential barrier, related to larger (mobility) gap of LGB tissue due to the alloying with H (and other "impurities" like O, C), which concentrates to these LGB.

Recent results, observed by Yoon [23] support this idea. Yoon has done annealing of μc-Si:H [23] and observed the substantial decrease of H content, accompanied by the increase of E_A above 0.5 eV. We have evaluated [10] from his data prefactor σ_0, which after annealing increased above the $100\,\Omega^{-1}cm^{-1}$ limit. He concluded that the grain boundaries have been modified, in our terminology annealing- induced decrease of H content lead to the annihilation of LGB.

Now we can explain the results in Figs. 5, 7 and 8. The unique $T_S = 100\,°C$ sample is just on the edge but there are no LGBs in it. Small increase or decrease of T_S lead to the increase of H content, see Fig. 8, LGBs are formed and the decrease of activation energy E_A and prefactor σ_0 is observed, see Fig. 7. The asymmetrical change of E_A and σ_0 around $T_S = 100\,°C$, as well as of both diffusion length and σ_{PH},

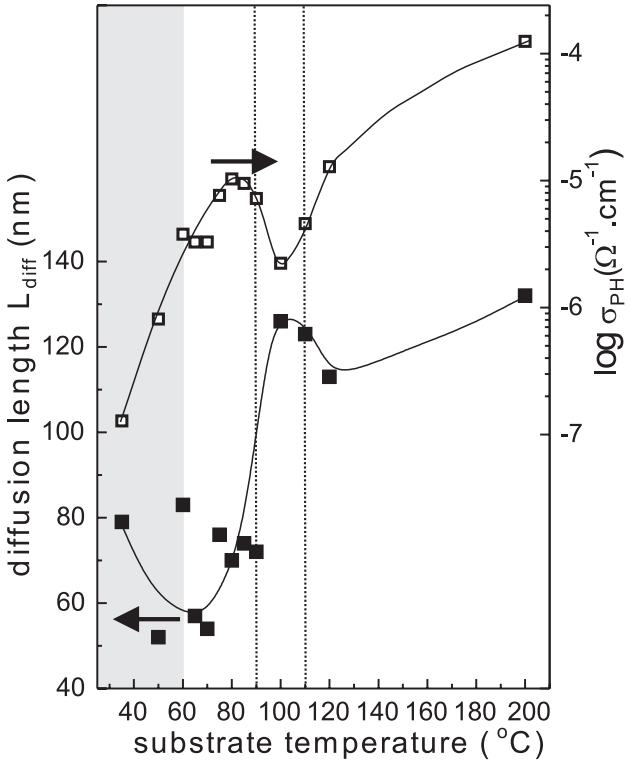

Fig. 9 Diffusion length L_{diff} from SSPG and photoconductivity (σ_{PH}) of sample series, prepared at 54 MHz and high dilution ($r_H = 134$) as a function of the substrate temperature T_S.

see Fig. 9, is related to the fact that while for $T_S > 100\,°C$ there is almost no change in crystallinity, for $T_S < 100\,°C$ the crystallinity slightly (about 5%) decreases, see Fig 5.

Last point which needs an explanation, is the clearly opposite behavior of diffusion length and σ_{PH}, observed in Fig. 9 and in a transition region also for $T_S = 60\,°C$ and $T_S = 80\,°C$ series, see Figs. 2 and 4. The probable reason is the fact that the σ_{PH} is controlled by majority carriers, while L_{diff} by minority carriers. These quantities are strongly and inversely dependent on the position of the Fermi level.

To summarize this part, we have illustrated that the peaks in L_{diff}, roughness and H content are together with the sharp changes of X_C, the σ_D, E_A and σ_0 the features, typical for a-Si:H/μc-Si:H transition region. We have found that even at $T_S = 35\,°C$ the crystallinity as high as 50% can be achieved. Dramatic changes of transport properties (L_{diff} ,σ_D and σ_{PH}) have been observed for μc-Si:H temperature series also outside the a-Si:H/μc-Si:H transition region ($90\,°C < T_S < 110\,°C$). We have proposed, in agreement with the recent independent result [23], that the H-induced changes of the grain boundaries can explain these observations.

4 Geometry of the μc-Si:H growth and its application aspects

The microstructure of μc-Si:H influences electronic transport on multiple scales: subnanometric (atomic composition and local arrangement), nanometric (crystalline grains and their boundaries) and submicron (large grain aggregates or columns). Further complication arises from the evolution of the structure and film properties with the growing film thickness [24].

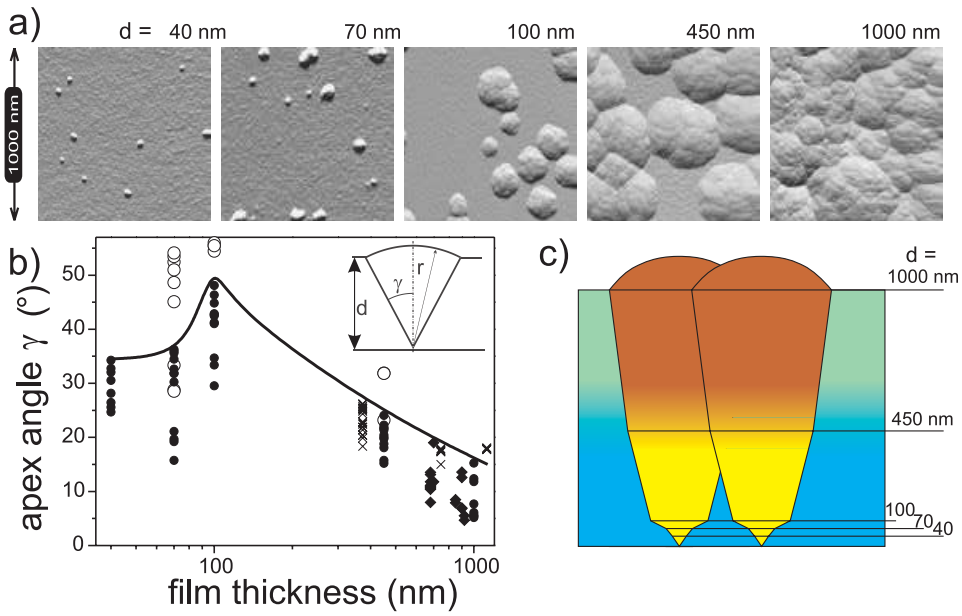

Fig. 10 In the top part the AFM morphologies are shown for the thickness series (a). The simplest possible shape of the grains would be a spherically capped cone with the apex angle γ shown in the inset of the graph (b). The apparent γ for a large number of grains for several thickness series as a function of the film thickness is plotted in the graph (b). The reconstruction of the grain shape evolution for the same series as shown in the top is then drawn in (c).

In the previous chapter 3 we have illustrated the changes of the μc-Si:H charge transport properties at the a-Si:H/μc-Si:H transition and explained them using the simple model using the concepts of density-of-states, transport path and the potential barrier at the "large grain boundaries" illustrated in Fig. 1. Here we want to point out that the experimentally observed properties such as the dark conductivity, photoconductivity, diffusion length are the effective properties in which the influence of the material structure is averaged over the whole sample. In this part we shall use a microscopic approach, looking into the details of the microstructure resulting from the growth. Then we shall explore how the geometrical description of the microstructure could be used to simulate the effective transport properties and discuss its possible application related aspects.

We have previously discussed a description of the μc-Si:H geometry based on the growth of grains in the Voronoi network of grain neighbourhoods [25]. The model was constructed on the basis of an AFM observation such as shown in the Fig. 10a) for a thickness series of the μc-Si:H samples. At the lowest thickness we have observed roughly circular isolated grains (in this part we use the term grain to denote the observed microcrystalline regions, although it should be kept in mind that they are in fact aggregates composed of nanometer sized subgrains [24]).

With the growing sample thickness the grains enlarge and collide, forming nearly straight boundaries. We have described the network of the grain boundaries by Voronoi tessellation [25] and used it to model the evolution of roughness and grain size [1]. The model assumed the simplest possible geometry shown schematically in the Fig. 10b) which assumes that the isolated grains grows as a spherically capped cone. Conical grain with a spherical cap would grow as a result of different growth rates v_a and v_c of the amorphous and (micro)crystalline surfaces. The cone angle γ (measured from the cone axis) is given by formula $\cos\gamma = v_a/v_c$.

We have later [26] reexamined this assumption by measuring the radii of a large number of grains observed on the surface of several thickness series of μc-Si:H samples (grown at low substrate temperatures). We have avoided smaller grains resulting from the late nucleation and assumed that the grains started to grow without an incubation layer and plotted the apparent apex angle γ vs. the thickness of the films in Fig. 10b. The apparent apex angle γ is not constant during the film growth, it first increases as the grains expand and then decreases again in so called elongation phase of the growth.

An idealized evolution of the grains for the thickness series of samples is shown in Fig. 10c), corresponding the the AFM images in the same figure. In the same study [26] it was observed that the grain caps may indeed be approximated by spherical cap (disregarding the finer roughness due to cauliflower structure), although the sphere centre did not coincide with the grain tip. The grain shape evolution should reflect the microscopic processes by which the growth precursors are incorporated into the growing grain or surrounding amorphous matrix [27], however, further study is needed to establish whether and how this may be used to extract an information about these processes from the grain shapes.

Simple analytic description of the mixed phase μc-Si:H geometry makes it easier to simulate the electric field distribution and thus also the transport of the charge carriers. While the Voronoi network corresponds to the cell boundaries, its dual, Delaunay triangulation, corresponds to the grain connections [28]. If we want to study electrical transport parallel to the substrate, the Delaunay edges point to the nearest neighbors of any grain and so they correspond to the most probable current path.

We can use the grain distance or the area of their boundary to find a resistance limiting the current flow between two nearest neighbors and then we calculate sample conductivity as a resistor network using the Kirchhoff's laws applied to the Delaunay network as an electrical circuit [29–31]. This approach has been used for simulating polycrystalline materials, for example ceramic multicrystals [32] and it was noted that the field inhomogeneities lead to the current concentration to filaments of the lowest resistance.

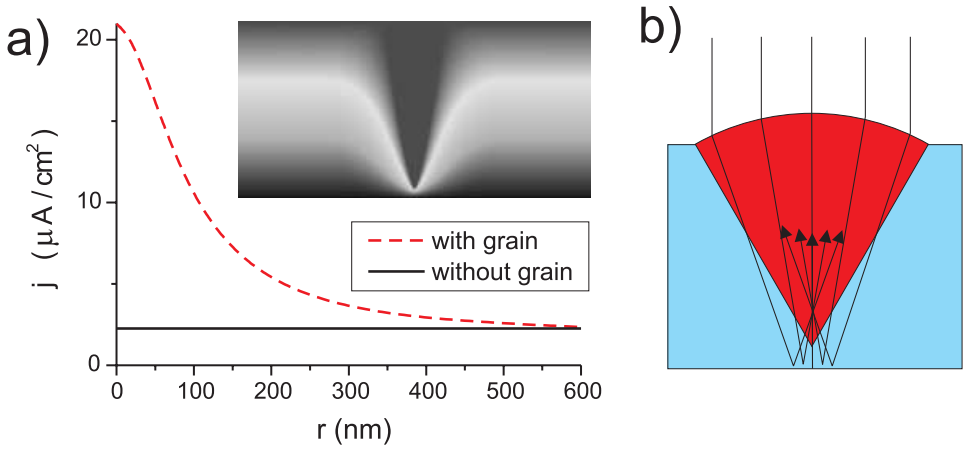

Fig. 11 Concentration of field and photogeneration to the grain tip. The plot (a) shows current density at the bottom electrode as a function of the radial distance from the grain axis. The currents were obtained from the numerical solution of the Laplace equation as shows in the inset. (b) A schematic illustration of the light concentration to the tip of the conical grain from the most simple ray tracing.

Even larger concentration of the electric field can be expected when the external bias is applied to the sandwich arrangement of electrodes, used also in solar cells. The conductivity of the grains is much higher than that of the amorphous silicon. If we cover the film with a top electrode and apply a voltage, the grain behaves almost as an equipotential and brings the potential of the top electrode much closer to the layer bottom interface. The drop of the applied potential on much smaller distance between the grain tip and the sample bottom contact will locally create much stronger electric field, which will be increased even

further by the sharpness of the tip. Concentrated electrical field will also increase the current density in the amorphous phase near the grain tip.

For example, we have numerically solved the electrostatics of the grain embedded in a 500 nm thick film with a 50 nm thick incubation layer as shown in the inset of the Fig. 11a). The grain was surrounded by an amorphous vicinity with the diameter 600 nm, corresponding to the surface crystallinity 18%. Using the values of conductivity $10^{-10}\,\Omega^{-1}\mathrm{cm}^{-1}$ for a-Si:H and $10^{-5}\,\Omega^{-1}\mathrm{cm}^{-1}$ for the grain (typical values for intrinsic device-grade a-Si:H and μc-Si:H), the presence of the grain leads to an increase of the current in sandwich samples about 2 times. Moreover, the current density at the bottom electrode (Fig. 11a) reaches a maximum at the grain tip where the field si concentrated about 20 times, and in fact, almost 60% of the total current passes through the sample under the grain — although it covers only 18% of the surface.

The concentration of the electric field near the grain tip may also coincide with the concentrated photogeneration of the carriers. Corrugation of the μc-Si:H surface leads to inherent light trapping and is usually described by the scattering factors [33], using an assumption of a random, non-correlated surface with typical features much smaller than the light wavelength. For grains with size comparable or surpassing the wavelength of visible light this assumption is no longer valid. Spherical surface of large enough grains may lead to at least partial light focussing as shown schematically in Fig. 11b). Coincidence of the electric field and photogeneration concentration, due to the growth of the grains with conical shapes, may result in a new principle of the solar cell operation [26].

5 Non-traditional preparation of polycrystalline silicon

It was reported that solid-phase crystallization temperature can be substantially decreased when certain metals are in contact with the a-Si:H precursor. In particular, nickel [34] and aluminium [35] turned out to be suitable for this purpose. Depositing a very thin Ni layer onto an a-Si:H film and, in addition, applying a dc electric field, the crystallization temperatures to as low as 500 °C [36] or even 380 °C [37] have been achieved. The electric field can thus also contribute to reducing the crystallization temperature and one speaks about electric-field-assisted MISPC.

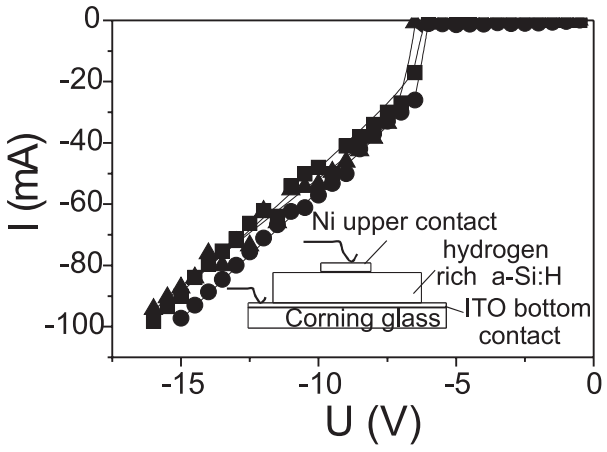

Fig. 12 Three examples of current-voltage plots measured on three different nickel contacts. Scheme of the device is shown in the inset. The polarity refers to the nickel electrode. The stepwise increase in current at -6.5 V indicates crystallization.

All preceding studies dealing with the electric-field-enhanced MISPC of a-Si:H used low electric fields of the order of 10 to 100 Vcm^{-1}, applied laterally via a pair of coplanar electrodes deposited to the a-Si:H films. We have shown recently that a-Si:H can get crystallized even at room temperature(!) [2, 38], provided that:

- the a-Si:H film contains high concentration of hydrogen (from 20 to 45 at. % H) and
- high electric field of the order of 10^5 Vcm^{-1} is applied in perpendicular to the substrate on which a-Si:H film is deposited.

Under these conditions, instantaneous or "explosive" crystallization occurs without any additional heating or laser illumination. Here we briefly review the main features of this phenomenon.

The structure (see Fig. 12) used for crystallization experiments has been prepared as follows. A Corning 7059 glass substrate has been covered with a thin film (about 350 nm) of transparent conductive oxide (indium tin oxide (ITO)) onto which the a-Si:H film has been deposited by plasma enhanced chemical vapor deposition using pure SiH_4 diluted strongly with helium. The substrate temperature T_S was kept as low as 50 °C instead of the usual 250 °C used commonly for device-grade a-Si:H film fabrication. Such low temperature together with the helium dilution of SiH_4 assured high hydrogen content in prepared a-Si:H [39]. The thickness of the a-Si:H films varied between 0.4 and 1.7 μm. On the top of the films, circular nickel electrodes with thickness of 40 nm and diameter of 1 to 3 mm were evaporated. The electric field was applied across the film between the top (Ni) and the bottom (ITO) electrodes using spring stainless steel contacts. All crystallization experiments have been performed at room temperature and ambient atmosphere.

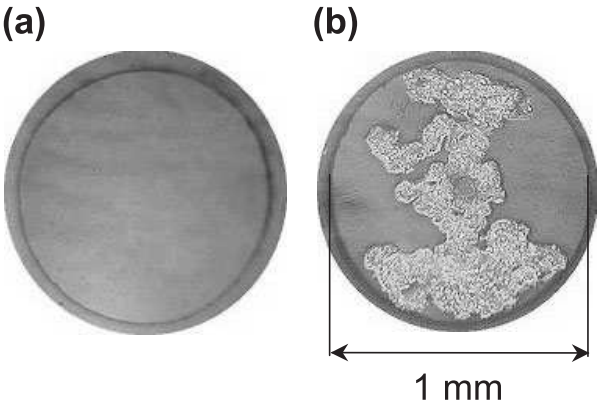

Fig. 13 Microscopic view of a virgin nickel contact before the crystallization step (a) and after the crystallization (b). The irregular island represents crystallized poly-Si.

We have obtained the first experimental manifestation of ongoing crystallization during the measurement of current-voltage curves on as-prepared samples. These curves are displayed in Fig. 12. At low voltages, the intact samples exhibit very low conductivity owing to the large bandgap of hydrogen rich a-Si:H. A striking increase in current occurs at approximately -6.5 V (the voltage polarity refers to the nickel electrode); the corresponding electric field across the a-Si:H film is about 1.6×10^5 Vcm^{-1}. By observing the sample simultaneously with an ordinary microscope, we found clear correlation between this sudden current rise and instantaneous appearance of a crystallized region in the sample.

Typical example of a microscopic view of a nickel contact is shown in Fig. 13. (We should note that this observation was performed "from below" by taking advantage of the good transparency of both ITO and hydrogen-rich a-Si:H to visible light.) The left view (a) represents a virgin Ni contact before reaching the "threshold" voltage of -6.5 V, while the right view (b) shows an irregular crystallized silicon island which

appeared always simultaneously with the stepwise rise in current (see Fig. 12). The crystalline nature of the island was evidenced, among others, by the X-ray diffraction technique [40] and by electroluminescence studies [38]. Here we present an example of micro-Raman investigation of the crystallized regions, together with information about the morphology and the crystalline volume fraction of resulting poly-Si [2].

The micro-Raman spectra were studied using a Renishaw 1000 system equipped with a Leica microscope (excitation wavelength 514 nm, spot diameter about 2 mm). Shown in Fig. 14 are the optical micrographs taken from the topside of the sample (left-hand column) and micro-Raman spectra (right-hand column) measured at points indicated by full circles on the line in the left part. Panel (a) represents results obtained in an as-prepared a-Si:H film. The micro-Raman lines are wide and peaked at about 480 cm^{-1} which is a very well known fingerprint of a-Si:H. The observed background in micro-Raman spectra is due to room temperature photoluminescence occurring in hydrogen-rich a-Si:H [41].

Panel (b) shows results obtained in a polycrystalline film prepared by applying a negative polarity electric field to a tiny patterned Ni contact. The difference to panel (a) is striking. Uniform-sized fine poly-Si grains with a mean size of ~ 3 mm can be recognized in the left column. Raman spectra in the right column contain narrow peaks at 520 cm^{-1}, characteristic of crystalline silicon. Virtually no photoluminescence background can be seen and the crystalline volume fraction achieves a value close to 100%.

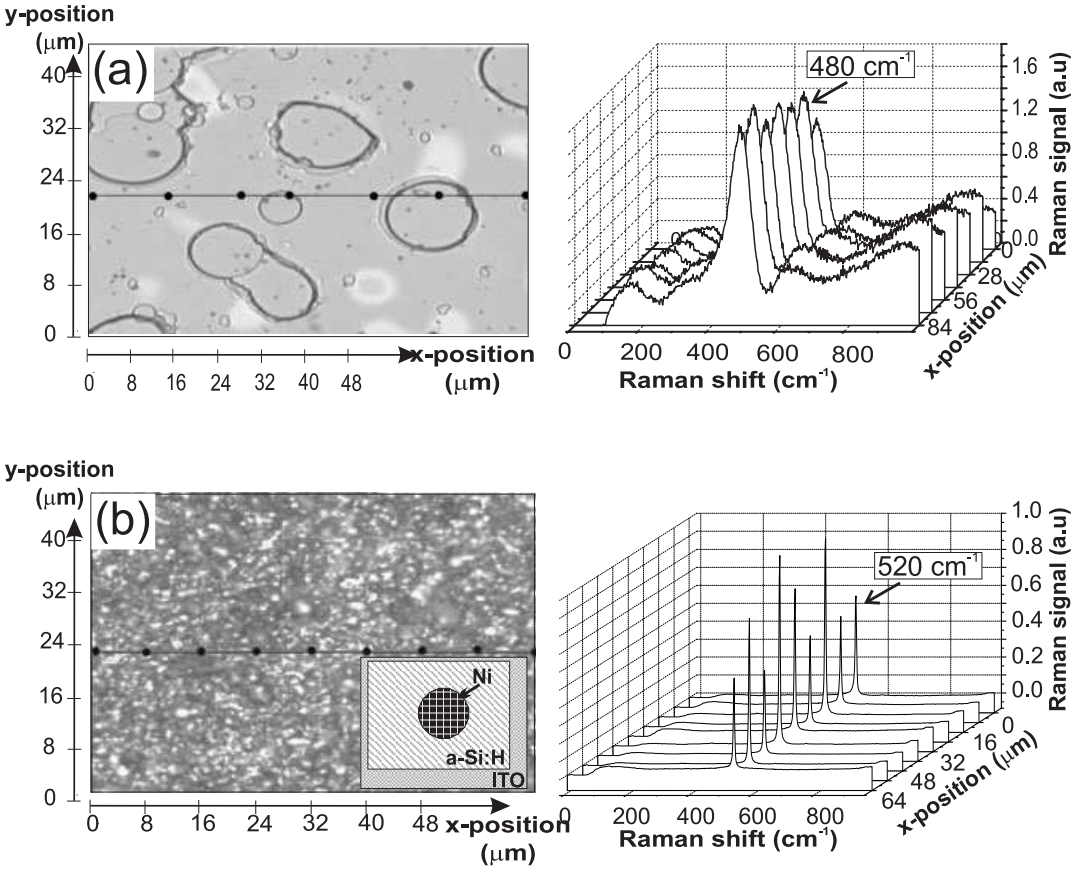

Fig. 14 Optical micrographs (left) and micro-Raman spectra (right) measured at points indicated by full circles on the line in the left part. (a) As prepared a-Si:H precursor. (b) crystallized poly-Si upon application of an electric field with negative polarity.

While we have tested empirically on a large number of samples that this explosive room-temperature electric-field-assisted MISPC works absolutely reliably, we understand the physics behind it qualitatively only. The process is obviously initiated by dielectric breakdown of the a-Si:H film at the threshold electric field of about 10^5 Vcm^{-1}. The accompanying Joule heat induces creation of nickel silicides Ni_2Si and $NiSi_2$, because these are formed at relatively low temperature (200 °C). The silicides then migrate through the a-Si:H matrix and represent effective nucleation sites for silicon crystallization since the lattice constant of $NiSi_2$ differs from that of crystalline silicon by 0.5% only. The whole process is kept going partially by exploiting the released latent heat of crystallization.

Of crucial importance appears the high hydrogen content in the a-Si:H precursor. Recently a theoretical model of hydrogen-induced crystallization of a-Si:H has been proposed [42]. The model demonstrates, using molecular-dynamics simulation, that crystallization is mediated by the insertion of H atoms into strained Si-Si bonds. Such H-insertion facilitates chemically (not thermally)-induced rearrangement of the a-Si:H network and allows crystallization even at very low temperatures, in full agreement with our experimental data.

Another supporting factor can be the presence of higher concentration of microscopic voids in the a-Si:H network containing more than 14 at. % of H, as established quite recently [43]. The nickel silicides can diffuse much more easily through a widely branching void network in an a-Si:H film with high hydrogen content. The progress of the crystallization front leads finally to eruption of hydrogen, which gives the process an explosive character.

Last but not least, the polarity of the applied voltage with respect to the Ni contact plays also a role. The onset of crystallization in Fig. 12 occurs at a negative polarity, and Fig. 13 and Fig. 14 are related also to a negative polarity. Achieving crystallization under a positive polarity turned to be more difficult. This observation correlates with the finding that nickel atoms in $NiSi_2$ carry probably a negative electric charge [36]. The Coulomb force then pushes the crystallization front across the whole film thickness, facilitating thereby full crystallization.

6 Possibility to use a-Si:H for "nanolitography"

PECVD preparation of a-Si:H and μc-Si:H is well established industrial technology. Of great interest are today hybrid organic — silicon devices, in which bio-active molecules could be arranged or even better self-organised on silicon interface without the complicated conventional technological steps and with the necessary (nm) resolution.

Contrary to μc-Si:H, which has rather complicated microstructure, a-Si:H is very homogeneous (namely a-Si:H prepared from pure undiluted SiH_4) down to few nm scale and so we could use it for the "nano-lithography" when the suitable recording method is at hand. Recently [13, 44] we have observed what we called "memory effect" during the AFM measurement. Consecutively [44, 45] we have studied this effect in detail as a function of AFM tip polarity, proposed a model and discussed the role of charge trapping and oxidation.

In Fig. 15 [46] it is demonstrated that for applied positive tip voltages the topography is unchanged and so oxidation can be excluded, while the profile of the surface potential (recorded by measuring in parallel Kelvin Force Microscopy — KFM) is changed, clearly indicating important role of metastable charge trapping. All experimental details and procedures are in detail described in [45, 46], important is that due to the low re-emission probability of the trapped charge the charge patterns persist for long enough time (up to 17 hours).

Moreover, by adjustment of the voltage pulse amplitude, contact force and the scan speed the potential difference as high as 0.8 V (close to theoretical limit), see Fig. 16, has been achieved [46] and it has been shown that the exposure to water (needed for biological applications) has no influence or even improves the contrast of the recorded charge patterns [46].

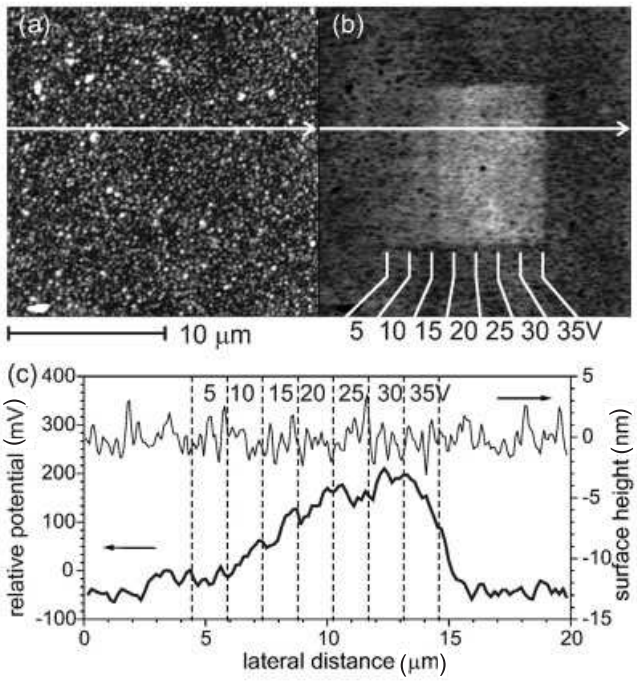

Fig. 15 (a) AFM surface topography (Z range 40 nm) and (b) surface potential (Z range 0.8 V) images of a-Si:H after the series of positive tip voltage pulses ($5 - 35$ V). (c) Corresponding line profiles acquired along the arrows in the images.

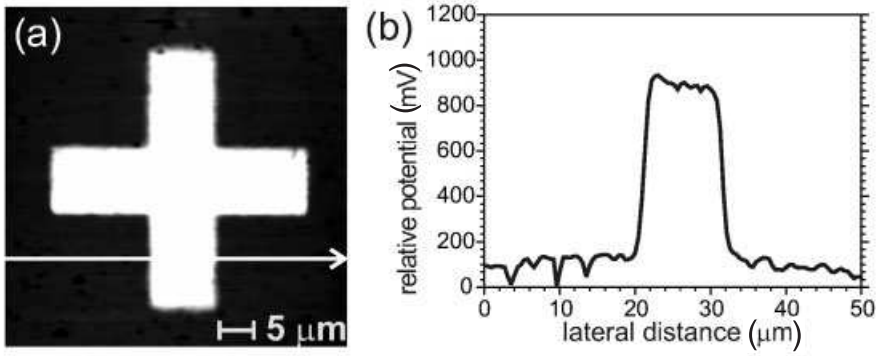

Fig. 16 (a) Kelvin force microscopy image of potential (Z range 0.8 V) of a-Si:H surface, where a cross-like charge pattern has been written using 60 V. (b) corresponding line profile across the pattern (acquired along the arrow in the image).

7 Conclusions

Silicon thin films prepared near the boundary between the a-Si:H and μc-Si:H growth not only offer superior properties for industrial applications (PV cells, thin film transistor arrays for LCDs), but

also an excellent opportunity for studying the role of hydrogen, grain boundaries and other factors decisive for the device performance. We have used four series of Si samples in which the a-Si:H/μc-Si:H boundary was crossed by changing a single technological parameter (dilution of silane in hydrogen, deposition temperature, sample thickness).

For each of the technological parameters there exists a threshold for a conductivity increase from the a-Si:H value $10^{-11}\,\Omega^{-1}\mathrm{cm}^{-1}$ to the μc-Si:H value above $10^{-7}\,\Omega^{-1}\mathrm{cm}^{-1}$. The difference between the threshold value of the deposition parameters for the conductivity transition and for the crystallinity transition has been observed, for very low substrate temperatures surprisingly large.

We have used a model of transport based on the concept of the potential barrier at the boundary of large ($100 - 300$ nm) grains (LGB) and its effect on the transport path for a unified description of the electronic transport. The model is able to explain all experimental data and was further supported by the increase of hydrogen content observed by ERDA at the a-Si:H/μc-Si:H transition region and also by a direct observation of the morphology and local electronic properties of the Si films using a conductive tip of AFM.

The surprising changes of the diffusion length and photoconductivity outside the a-Si:H/μc-Si:H transition region, observed for the temperature series, have been clearly related to the H content and their opposite changes explained by the Fermi level shift.

Macroscopic electronic transport measurements result in effective parameters, influenced by the grain boundaries, amorphous tissue and barriers averaged over the whole sample. In order to gain a microscopic understanding we have discussed the geometrical model of mixed phase Si which can be used for transport simulation. We have pointed out the presence of electric field inhomogeneities. We have also noted that for large grains (with sizes reaching up to $1\ \mu$m) the spherical caps may concentrate the photogeneration to region with an enhanced electric field near the grain tip.

We have devoted special attention to the deposition at low substrate temperatures as a reaction to the current demand for the use of cheap plastic substrates. We have also pointed out the results of an alternative, low temperature way of preparing polycrystalline Si films by the metal-induced crystallization of a-Si:H supported by the electric field.

Finally, we have illustrated how the vast amount of the technological know-how for a-Si:H and μc-Si:H may find a new use in future applications by using an example of possible nanolithography, which uses the AFM tip to inject electronic charge into the surface of a-Si:H.

Acknowledgements This research was supported by projects AVOZ1010914, GA AV IAA1010316, B2949101, VaV 300/01/03 and and GA ČR 202/03/0789. We would like to thank Walther Fuhs for many stimulating discussions which we had at different occasions not only on scientific subjects.

References

[1] T. Mates, A. Fejfar, I. Drbohlav, B. Rezek, P. Fojtík, K. Luterová, J. Kočka, C. Koch, M. B. Schubert, M. Ito, K. Ro, and H. Uyama, J. Non-Crystal. Solids **299–302**, 767 (2002).
[2] P. Fojtík, K. Dohnalová, T. Mates, J. Stuchlík, I. Gregora, J. Chval, A. Fejfar, J. Kočka, and I. Pelant, Phil. Mag. B **82**, 1785 (2002).
[3] T. Sameshima, M. Hara, and S. Usui, Jpn. J. Appl. Phys. **28**, 1789 (1989).
[4] K. Winer, G. B. Anderson, and S. E. Ready, Appl. Phys. Lett. **57**, 2222 (1990).
[5] K. Nakazawa, J. Appl. Phys. **69**, 1703 (1991).
[6] T. E. Dyer, J. M. Marshall, and J. F. Davies, Phil. Mag. B **69**, 509 (1994).
[7] A. Yin and S. J. Fonash, J. Vac. Sci. Technol. A **12**, 1237 (1994).
[8] Y. Masaki, P. LeComber, and A. Fitzgerald, J.Appl. Phys. **74**, 129 (1993).
[9] A. Fejfar, T. Mates, P. Fojtík, M. Ledinský, K. Luterová, H. Stuchlíková, I. Pelant, J. Kočka, V. Baumruk, A. Macková, M. Ito, K. Ro, and H. Uyama, Jpn. J. Appl. Phys. **42**, L987 (2003).
[10] J. Kočka, A. Fejfar, P. Fojtík, K. Luterová, I. Pelant, B. Rezek, H. Stuchlíková, J. Stuchlík, and V. Švrček, Solar Energy Materials & Solar Cells **66**, 61 (2001).
[11] J. Kočka, T. Mates, P. Fojtík, M. Ledinský, K. Luterová, H. Stuchlíková, J. Stuchlík, I. Pelant, A. Fejfar, M. Ito, K. Ro, and H. Uyama, ICAMS20 (Campos do Jordao 2003), to appear in J. Non-Crystal. Solids.

[12] U. Kroll, J. Meier, A. Shah, S. Mikhailov, and J.Weber, J. Appl. Phys. **80**, 4971 (1996).
[13] B. Rezek, J. Stuchlík, A. Fejfar, and J. Kočka, Appl. Phys. Lett. **74**, 1475 (1999).
[14] J. Meier, R. Flückiger, H. Keppner, and A. Shah, Appl. Phys. Lett. **65**, 860 (1994).
[15] J. Kočka, H. Stuchlíková, J. Stuchlík, B. Rezek, T. Mates, V. Švrček, P. Fojtík, I. Pelant, and A. Fejfar, J. Non-Crystal. Solids **299–302**, 355 (2002).
[16] J. Kočka, J. Stuchlík, H. Stuchlíková, V. Švrček, P. Fojtík, T. Mates, K. Luterová, and A. Fejfar, Appl. Phys. Lett. **79**, 2540 (2001).
[17] J. H. Werner and N. Christensen: in Polycrystalline Semiconductors II, Springer Proceedings in Physics, vol. **54**, edited by J. H. Werner and H. P. Strunk (Springer, Berlin, 1991), p. 145.
[18] T. Kamei, T. Wada, and A. Matsuda, MRS Symp. Proc. **664**, A.10.1.1 (2001).
[19] F. Finger, J. Muller, C. Malten, R. Carius, and H. Wagner, J. Non-Crystal. Solids **266–269**, 511 (2000).
[20] P. Kanschat, K. Lips, and W. Fuhs, J. Non-Crystal. Solids **266–269**, 524 (2000).
[21] M. Chukichev, P. Forsh, W. Fuhs, and A. G. Kazanskii, ICAMS20 (Campos do Jordao 2003), to appear in J. Non-Crystal. Solids.
[22] T. Mates, A. Fejfar, M. Ledinský, K. Luterová, P. Fojtík, H. Stuchlíková, I. Pelant, J. Kočka, A. Macková, M. Ito, K. Ro, and H. Uyama, Proc. of the 3rd World Conference on Photovoltaic Energy Conversion,May 2003,Osaka.
[23] J. Yoon, MRS Symp. Proc. **664**, A.23.6.1. (2001).
[24] J. Kočka, H. Stuchlíková, J. Stuchlík, B. Rezek, V. Švrček, P. Fojtík, I. Pelant, and A. Fejfar, Solid State Phenomena **80–81**, 213 (2001).
[25] A. Fejfar, T. Mates, C. Koch, B. Rezek, V. Švrček, P. Fojtík, H. Stuchlíková, J. Stuchlík, and J. Kočka, Mat. Res. Soc. Symp. Proc., Vol. **664**, A16.1.1 (2001).
[26] A. Fejfar, T. Mates, O. Čertík, B. Rezek, J. Stuchlík, I. Pelant, and J. Kočka, ICAMS20 (Campos do Jordao 2003), to appear in J. Non-Crystal. Solids.
[27] G. S. Bales and A. Zangwill, J. Vac. Sci. Tech. A **9**, 145 (1991).
[28] A. Okabe, B. Boots, and K. Sugihara, Spatial Tessellations: Concepts and Applications of Voronoi diagrams (J. Wiley & Sons, New York, 2000).
[29] C. Donolato, Semicond. Sci. Technol. **15**, 15 (2000).
[30] M. Bartkowiak and G. Mahan, Phys. Rev. B **51**, 10825 (1995).
[31] T. Nagaya and Y. Ishibashi, Jpn. J. Appl. Phys. **37**, 157 (1998).
[32] J. Fleig, Solid State Ionics **150**, 181 (2002).
[33] A. Poruba, A. Fejfar, Z. Remeš, J. Špringer, M. Vaněček, J. Kočka, J. Meier, P. Torres, and A. Shah, J. Appl. Phys. **88**, 148 (2000).
[34] C. Hayzelden and J. L. Batstone, J. Appl. Phys. **73**, 8279 (1993).
[35] O. Nast, S. Brehme, S. Pritchard, A. Aberle, and S. Wenham, Solar Energy Materials & Solar Cells **65**, 385 (2001).
[36] J. Jang, J. Y. Oh, S. K. Kim, Y. J. Choi, S. Y. Yoon, and C. O. Kim, Nature **395**, 481 (1998).
[37] S. Y. Yoon, J. Y. Oh, C. O. Kim, and J. Jang, J. Appl. Phys. **84**, 6463 (1998).
[38] I. Pelant, P. Fojtík, K. Luterová, J. Kočka, A. Poruba, and J. Štěpánek, Appl. Phys. A **74**, 557 (2002).
[39] K. Luterová, I. Pelant, P. Fojtík, M. Nikl, I. Gregora, J. Kočka, J. Dian, J. Valenta, P. Malý, J. Kudrna, J. Štěpánek, A. Poruba, and P. Horváth, Phil. Mag. B **80**, 1811 (2000).
[40] I. Pelant, P. Fojtík, K. Luterová, J. Kočka, K. Knížek, and Štěpánek, Thin Solid Films **383**, 101 (2001).
[41] J. Dian, J. Valenta, J. Hála, A. Poruba, P. Horváth, K. Luterová, I. Gregora, and I. Pelant, J. Appl. Phys. **86**, 1415 (1999).
[42] S. Sriraman, S. Agarwal, E. S. Aydil, and D. Maroudas, Nature **418**, 62 (2002).
[43] A. Smets, W. Kessels, and M. van de Sanden, Appl. Phys. Lett. **82**, 1547 (2003).
[44] B. Rezek, T. Mates, E. Šípek, J. Stuchlík, A. Fejfar, and J. Kočka, J. Non-Crystal. Solids **299–302**, 360 (2002).
[45] B. Rezek, T. Mates, J. Stuchlík, J. Kočka, and A. Stemmer, Appl. Phys. Lett. **83**, 1764 (2003).
[46] B. Rezek, J. Stuchlík, J. Kočka, and A. Stemmer, submitted to J. Non-Crystal. Solids.